

Original Research Article

Mechanical Structure Design and Optimization of a Humanoid Robot Arm for Education

Kevin Morales*, Carlos Hoyos, Jesús M. García

Laboratorio de Prototipos, Decanato de Investigación, Universidad nacional experimental del Táchira, Venezuela

ABSTRACT

This paper introduces the mechanical structure design and construction of a four degree of freedom humanoid robot arm for teaching purposes. The project started from the concept development stage and obtained six suggestions to meet the needs of customers. Then, the concept to be developed is selected according to the product specification. For the proposed concept, seven redesign phases were carried out to achieve the final design proposal. Specifically, continuous simulation steps are carried out to analyze the dynamic response of the structure under load, observe the stress state of each component, and adjust the size of the connecting rod according to the previously defined constraints and specifications. Based on the results obtained, a structure conforming to the original design specification is generated, taking into account the limitations related to the servo motor to be used and the maximum load to be handled. Finally, the kinematics models of the straight arm and reverse arm of the developed product are given.

Keywords: Manipulator Anthropomorphic Arm; Mechanical Design; Educational Robot

ARTICLE INFO

Received: Mar 21, 2022

Accepted: May 6, 2022

Available online: May 13, 2022

*CORRESPONDING AUTHOR

Kevin Morales

kevin.morales@unet.edu.ve;

CITATION

Morales K, Hoyos C, García JM. Mechanical structure design and optimization of a humanoid robot arm for education. Journal of Autonomous Intelligence 2022; 5(1): 95-109. doi: 10.32629/jai.v5i1.510

COPYRIGHT

Copyright © 2022 by author(s) and Frontier Scientific Publishing. This work is licensed under the Creative Commons Attribution-NonCommercial 4.0 International License (CC BY-NC 4.0).

<https://creativecommons.org/licenses/by-nc/4.0/>

1. Introduction

At present, robot technology is one of the most advanced research and development fields in the technical field. At present, robots are engaged in different work fields (robot arms with different end effectors)^[1,2] and various working environments, such as medical rehabilitation^[3], agriculture^[4], planetary exploration^[5], search and rescue^[6], military activities^[7] and entertainment parks^[8], cinemas^[9] and museums^[10]. Therefore, it is important to provide the University of science and technology with the latest knowledge in this field, as many professionals will be included in the growing field of robotics. In addition, from the perspective of pedagogy, educational robot is a great tool, which enables individuals to “give full play to all the exploration and operation abilities of cognitive subjects to serve the construction of meaning according to their own educational experience”^[11]. Therefore, robotics is a useful tool not only in technology, but also in pedagogy. Therefore, many basic education institutions use educational robots as a means to awaken students’ cognitive ability in a more effective way than traditional teaching methods^[12].

On this basis, the design of a 4GDL humanoid robot arm is proposed to meet some requirements of the Prototyping Laboratory of the Universidad Nacional Experimental del Táchira, Venezuela. The laboratory needs a low budget robot arm to develop its research projects, such as developing and improving single joint and multi joint control systems for trajectory tracking, Vibration control and development of small work unit with arm as actuator. In addition, it will also be used in laboratory

practice, such as characterization of robot kinematics and dynamics modeling, trajectory tracking in Cartesian space, programming and definition of manipulator accuracy, repeatability and resolution. In addition, due to the required characteristics, the designed arm can become a useful tool for robotics teaching in primary and secondary schools.

In order to start the project, the design of robot arm is studied from different angles. A manipulator design and structure using a simple method is proposed, which emphasizes the conceptual selection of sensors and actuators to determine the connecting rod size and estimate the bearing capacity of actuators^[13]. Considering the use of arm kinematics research to determine the connecting rod size, the design and structure of 5GDL robot arm are proposed^[14]. A control system based on mechanical structure is developed, which is developed according to the dimension design standard in CAD modeling^[15]. Product development technologies such as QFD (Quality Function Development) are used to design robot arms^[16]. Finally, a simple manipulator model is developed^[17]; the vibration characteristics of the manipulator are studied by finite element method, and the static stress and buckling analysis are carried out at four important positions considered by the designer.

In this article, we introduce the development of the mechanical structure of a 4GDL humanoid robot arm. It uses a complete methodology, which brings together the advantages of the previously written methodology, but has two substantive contributions. The first method is to use dynamic simulation (mechanical event simulation) rather than static simulation to analyze the critical position of the arm when handling the maximum load; Therefore, the stress analysis of each arm link is carried out in the most dangerous position to ensure the strength of the arm within the range of available positions in its working load. The second input involves a process of adjusting and optimizing the quality of the connecting rod, taking into account the results of the connecting rod stress analysis obtained at each redesign stage and the torque applied to the actuator.

2. Method

For the design of humanoid robot arm, the product development method specified^[18] is used, which starts with defining customer needs in the interview and investigation of the end users of the arm. The identified requirements are then used to determine the required design specifications. On this basis, the definition process of various conceptual models is carried out to meet the previously specified requirements. At this stage, six proposals have been identified and will move on to the next design stage.

Then, a concept selection stage is proposed to select the appropriate concept according to the product specification (in the six proposals that have been defined). Select the concept to be developed and carry out different stages of redesign (sizing) and optimization to obtain the final structure and meet the limitations specified in the target specification.

In this iterative stage, the kinematics, dynamics (mechanical event simulation) and stress analysis of the arm are carried out to obtain the response of the structure and actuator to the load applied on the end actuator. After each analysis, the arms were sized to reduce mass to make the structure more dimensionally efficient, fail free under operating conditions, and can be driven by available and feasible structural actuators. Then it introduces the design process of the 4GDL humanoid robot arm and the results after redesign and optimization.

3. Result

3.1. Select concepts to develop

3.1.1. Design code

In order to develop the design specifications that the proposed robot arm should meet, it is necessary to collect untreated customer needs through interviews and surveys with end users of the product. This information is recorded and expressed in appropriate technical language to obtain an interpreted customer voice. Then it determines the priority of requirements and determines the importance level of each requirement. Then the design index or target specification of the robot arm is established. These indicators are responsible for determining the extent

to which products meet customer needs. It is important to note that each indicator meets one or more identified needs. **Table 1** lists the target specifications of the products to be designed and their re-

spective units, acceptability of ideal value (V.I.) and marginal value (V.M.) and their importance in the range of 1 to 5, of which (1) is not important and (5) is very important:

Table 1. Objective specification of a robot arm

Metric No.	Metric	Unity	V.I	V.M	Importance
1	Workload	kg	>0.3	>0.05	5
2	Maximum range	m	>1	>0.4	5
3	Total mass	kg	<6	<12	4
4	Time required for manufacturing	h	<36	<40	3
5	Time required for maintenance	h	<0.5	<1	3
6	Parts cost	Bs	<500,000	<600,000	3
7	End effector interchangeability	Subj**	5	>3	4
8	Beautiful appearance	Subj**	>3	>1	2
9	Shipping capacity	Subj**	5	>3	4
10	Stiffness relative to ideal position	mm	<10	<15	5
11	Part safety factor	Adim*	>1.5	>1.2	5
12	Volume of work	m ³	>0.2	>0.01	5

Note: *Dimensionless unit; **Subjective unit on an evaluation scale from 1 to 5.

Source: self compiled.

Table 2. Based on the concept of internal function of robot arm, the matrix is generated

Function	Option 1	Option 2	Option 3			
Transmission: First joint						
	Gears	Bands	Direct*			
Transmission: Second joint						
	Gears	Bands	Direct*			
Transmission: Third joint						
	Gears	Bands	Direct*			
Transmission: Fourth joint						
	Gears	Bands	Direct*			
End effector connection						
	Flange	Plate				
Concept	No. 1	No. 2	No. 3	No. 4	No. 5	No. 6

Note: *Means that the servo motor is directly connected to the joint

Source: self compiled.

3.1.2. Concept generation

After determining the target specifications, some conceptual suggestions conforming to these specifications are produced. This enables us to de-

velop a wide variety of design solutions in order to choose the most appropriate choice. These recommendations are derived from a concept generation matrix (based on the internal functions of the robot

arm, see **Table 2**), which proposes different options for the power transmission system at the arm joints.

Then, different combinations were made between the proposed options (**Table 2**) to generate six concepts (**Figure 1**), including possible configurations for building 4 GDL robot arms that meet product specifications. For example, for concept 3, power transmission is achieved by connecting the servo motor directly to the connector, while concept 4 uses three available power transmission systems: gears (first and fourth connectors), direct coupling of the servo motor to the connector (second connector) and gaskets (third connector).

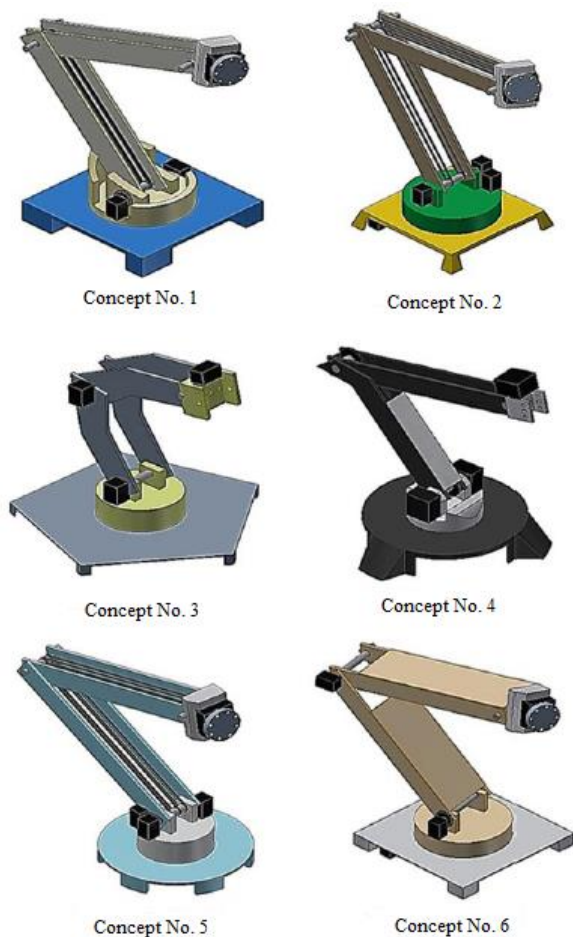


Figure 1. Generated concepts. Source: self compiled.

3.1.3. Select concepts to develop

When selecting alternatives to development, some criteria are used to assess the extent to which the generated concept meets the specifications defined for the product. Two selection stages are used. The first is a qualitative evaluation through the ma-

trix shown in **Table 3**, where each concept is evaluated according to the specifications previously developed using its marginal value. The reference codes used are as follows: (+) “ratio”, (0) “equal to”, (–) “ratio”. On the basis of this preliminary assessment, concepts 2, 3, 5 and 6 were excluded.

Subsequently, a weighted quantitative assessment was carried out with an assessment scale of 1 to 5 to distinguish the remaining concepts (1 and 4) according to the same specifications as above. This assessment is summarized in

Table 4 shows a matrix in which concept 6 is selected as the highest level according to the weights performed.

3.1.4. Description of the selected concept

The concept to be developed (option 4) should have the following characteristics:

- 4 GDL, each with four rotating joints (**Figure 2**).
- Housing structure of 4 servo motors and their power transmission system
- The servo motor is connected to the first connector through a gear.
- The servo motor is directly coupled to the second connector.
- The servo motor is connected to the third joint through the synchronous belt, and the servo motor is located on the first connecting rod.
- The servo motor is connected to the fourth joint through a gear, and the servo motor is installed on the third connecting rod.
- Claw end effector, driven by servo motor.
- Aluminum is selected as the material for designing connecting rods and other mechanical structural components.
- With a load of 1 N, the end effector can be manipulated.
- Servo motor control card space.
- A structure with a design factor (margin) of 1.2. This criterion also applies to the selection of actuators.
- End user arm obtained before using servo motor and other mechanical elements (gears).

Table 3. Qualitative matrix of concept evaluation

Selection criteria	Concept					
	01	02	03	04	05	06
Workload	+	+	-	+	+	-
Maximum range	+	+	+	+	+	+
Total mass	0	0	-	0	+	-
Time required for manufacturing	0	-	+	0	-	0
Time required for maintenance	0	-	+	0	-	0
Parts cost	0	0	0	0	0	0
End effector interchangeability	+	+	+	+	+	+
Beautiful appearance	+	0	0	+	0	0
Shipping capacity	0	0	0	0	0	0
Stiffness relative to ideal position	0	0	0	0	0	0
Part safety factor	+	+	+	+	+	+
Workload	0	0	+	+	0	+
Net evaluation	5	2	4	6	3	2
Continue?	Yes	No	No	Yes	No	No

Source: self compiled.

Table 4. Quantitative matrix of concept evaluation

Selection criteria	Weight (%)	Concept			
		01		04	
		Grade	Weighting	Grade	Weighting
Workload	10.4	5	0.52	5	0.52
Maximum range	10.4	5	0.52	5	0.52
Total mass	8.3	3	0.24	4	0.33
Time required for manufacturing	6.2	3	0.18	3	0.18
Time required for maintenance	6.2	3	0.18	3	0.18
Parts cost	6.2	3	0.18	3	0.18
End effector interchangeability	8.3	4	0.33	4	0.33
Beautiful appearance	4.1	2	0.08	3	0.12
Shipping capacity	8.3	3	0.24	3	0.24
Stiffness relative to ideal position	10.4	4	0.41	4	0.41
Part safety factor	10.4	5	0.52	5	0.52
Workload	10.4	4	0.41	4	0.41
Total			3.81		3.94
Continue?			No		Yes

Source: self compiled.

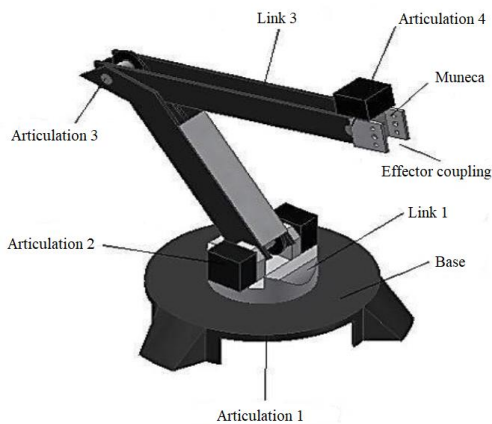


Figure 2. The final mechanical structure is obtained according to the selected concept. Source: self compiled.

3.2 Size and optimization of the obtained mechanical structure

The final mechanical structure was obtained after six improvements to the initial design, which was redesigned and optimized (**Figure 3**). In the first three designs, the focus is to adjust the structural size to obtain a suitable arm, which can meet the size specification, low mass and inertia, and can accommodate servo motor and power transmission elements. From redesign 4 to redesign 7, dynamic simulation was carried out to determine whether the torque required by the joint is below the allowable

limit (Table 5), taking into account that each joint has an available servo motor. In addition, a stress analysis was performed using MEF to verify the strength of each component when handling loads at critical locations. Based on these two analyses, the size of each connecting rod is adjusted to reduce the mass and torque applied to the actuator (Figure 4). This optimization is carried out in the area where the stress concentration of the part is low, so it will not affect the structural integrity of the part. In addition, it must be noted that the reduction in quality continues until the stress concentration is considerable or the new size and geometry of the part make the manufacturing process very difficult.

Finally, the final design (proposed 7ma) was obtained, which met the target specification and produced an appropriate torque that did not exceed

the allowable value of the available servo motor (Figure 5).

Then, through the dynamic simulation of the final designed joint and the stress analysis of its most key components, the results are obtained.

3.3 Dynamic simulation of determining arm structure

Dynamic simulation allows quantitative analysis of the position, velocity, acceleration and torque distribution of each component and joint when the structure moves by manipulating the maximum working load (1 N on the end effector). In order to perform this simulation on the joint, it is necessary to define the path of the mechanism and the velocity profile followed by the actuator related to the joint.

Table 5. Comparison between torques obtained through simulation for different design improvements

Articulation	Torque obtained (N-mm)			Maximum torque
	T _{design 5}	T _{design 6}	T _{design 7}	
1	34.5	18.9	15.5	302.5
2	2,096.0	2,020.0	2,005.6	2,019.2
3	655.5	622.7	757.4	777.4
4	8.7	5.4	3.7	394.0

Source: self compiled.

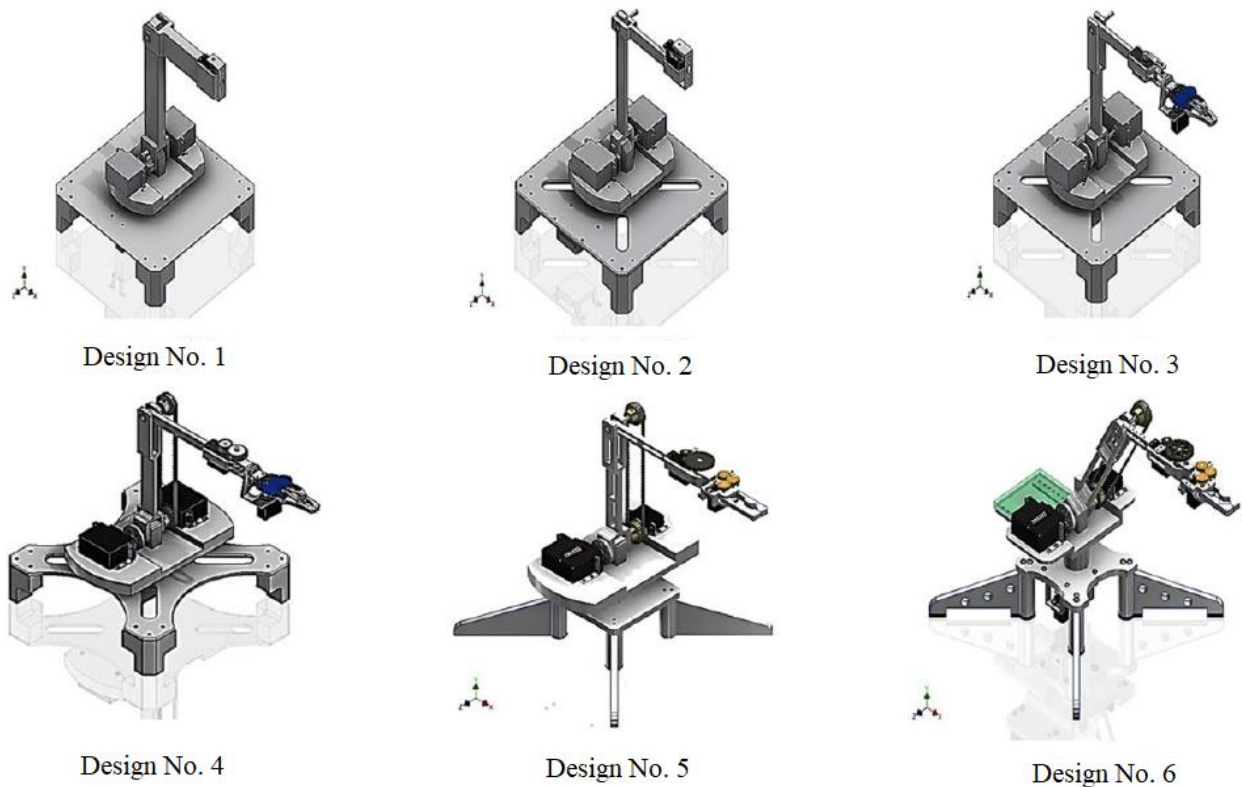


Figure 3. Design before obtaining the final design. Source: self compiled.

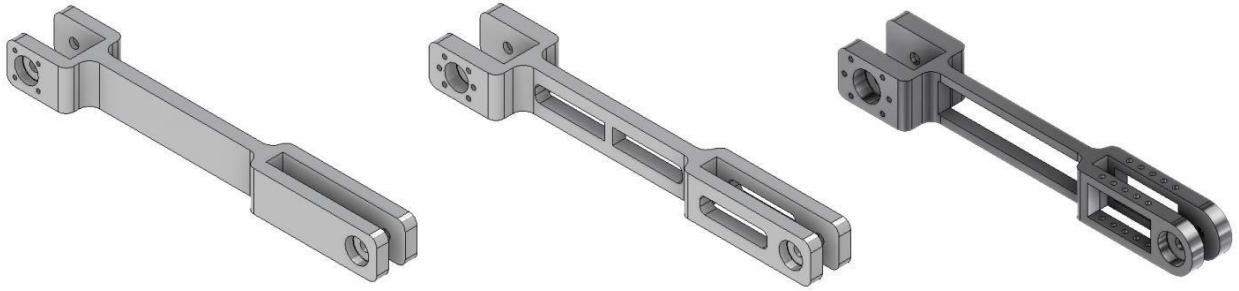


Figure 4. Evolution of link No. 2 for the last three stages of design and optimization. Source: self compiled.

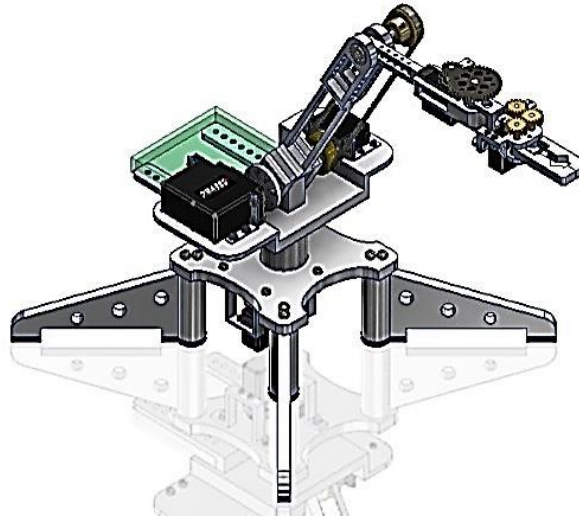


Figure 5. Final design of the robot arm (7th proposed design). Source: self compiled.

In the definition of speed profile, the speed profile is used for permanent speed, that is, the maximum available speed that the servo motor can provide when using its allowable torque. However, it is also important to define the velocity profile at actuator start-up, as this moment may be critical, depending on the position of the connecting rod. In order to define this profile, it is necessary to use the time constant of the actuator^[19], which takes into account the characteristics of the engine and the inertia characteristics of the servo motor and load transmission. For this purpose:

$$t_m = \frac{(J_I + J_r)R_m}{K_m^2} \quad (1)$$

where,

J_I = Moment of inertia of load, determined by:

$$J_I = J_{mec} + J_{eng}$$

J_{mec} = Moment of inertia of mechanism

J_{eng} = Moment of inertia of gearbox

J_r = Moment of inertia of servo motor

R_m = Measure the resistance on the servo motor

K_m = Mechanical constant, determined by:

$$K_m = \frac{R_m T_{bloq}}{V_{bloq}} \quad (2)$$

where,

T_{bloq} = Maximum torque of servo motor

V_{bloq} = Servo motor locking voltage.

The first joint is dynamically simulated according to the velocity profile defined by the arm inertia information provided by the CAD software using the technical data available by the hs-322hd servo motor (actuator of the first joint) and structural modeling (**Figure 6a**). This profile defines the angular displacement of the first joint in unidirectional and reverse motion (**Figure 6c**). It is worth noting that the previous purpose was to connect the servo motor directly to the axis of the first joint. In this case, the required torque is lower than the allowable torque of the actuator. However, the starting speed proved to be too slow, so a gear transmission system

was adopted to reduce the torque requirements of the servo motor. In this case, the maximum torque required is 15.5 N-mm (**Figure 6d**), which is lower than the allowable value of 302.5 N-mm servo motor (see **Table 5**). Although the size of the servo motor is too large, it ensures the quick start of the connector.

For the second connector, the servo motor used is hs-805bb, and the maximum torque value is 2019.2 N-mm. When the servo motor is directly installed on the joint, the speed profile defined for the actuator (**Figure 7a**) is dynamically simulated. The maximum torque value of 2005.6 N-mm (**Figure 7d**) was obtained to verify that the torque generated by the structure at the joint does not exceed the maximum torque defined for the servo motor.

The same is true of the third joint. In this case, the servo motor used corresponds to Futaba S9206, and the maximum torque value is 777.4 N-mm. The servo motor is located on the connecting rod 1. The belt transmission system and pulley are used to transmit power to the third joint, and the transmission ratio is 1. For the speed profile determined according to the characteristics of the servo motor and its load (**Figure 8a**), the maximum torque value obtained through dynamic simulation is 757.4 N-mm (**Figure 8d**), which is less than the maximum torque value allowed by the servo motor.

Finally, the dynamic simulation of the fourth joint is described, which is based on the speed profile

defined according to the characteristics of the available servo motor (HS-225BB) of the joint (**Figure 9a**), which transmits torque to the wrist shaft through the gear transmission system. The allowable torque value of the servo motor is 394 N-mm. According to the simulation, the maximum torque value required by the actuator is 4 N-mm (**Figure 9d**), which is less than the maximum allowable torque value. In this case, it can be said that the torque required by the servo motor relative to the application is too large, but it must be remembered that all the loads applied to the end effector (the weight of the manipulation load plus the weight of the claw) are supported by the wrist. Therefore, the actuator only needs to apply the torque required to move the wrist from left to right, which greatly reduces the torque required to perform this movement.

3.4 Stress analysis of main boom parts

The data obtained from dynamic simulation can define the critical position where the actuator must apply the maximum torque for each joint to achieve appropriate motion according to the required speed and trajectory profile. Given these critical positions, various stress analyses (MEFs) were performed on the arm components, including the load profiles obtained from the dynamic simulation of these critical positions.

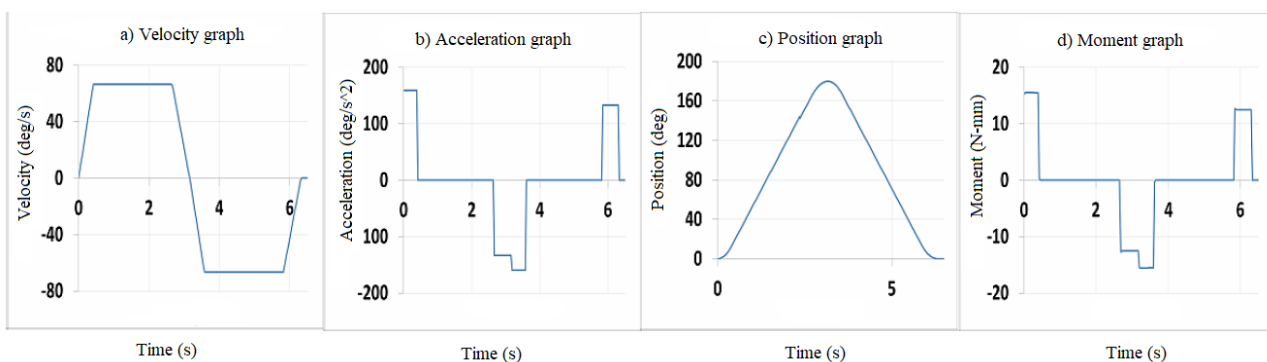


Figure 6. The dynamic simulation results of the servo motor coupled to the first joint (HS-322HD) are obtained. Profile: (a) velocity, (b) acceleration, (c) position and (d) moment. Source: self compiled.

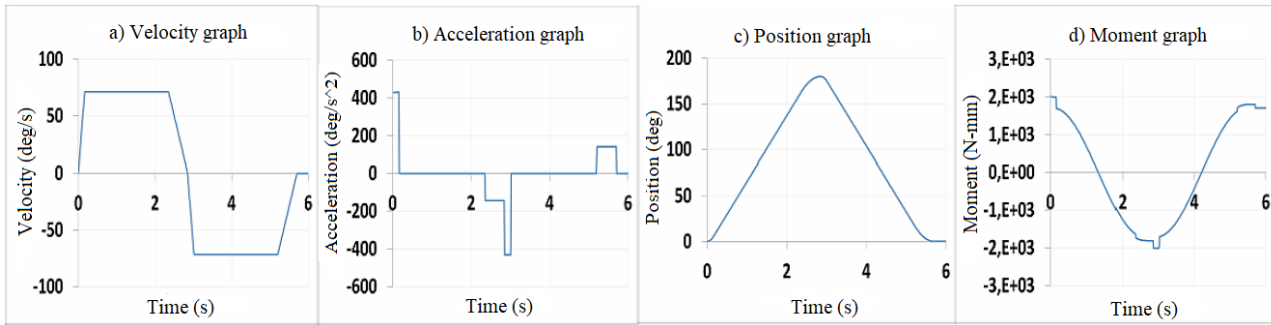


Figure 7. The dynamic simulation of the second joint is carried out by using hs-805bb servo motor, and satisfactory results are obtained. Profile: (a) velocity, (b) acceleration, (c) position and (d) moment. Source: self compiled.

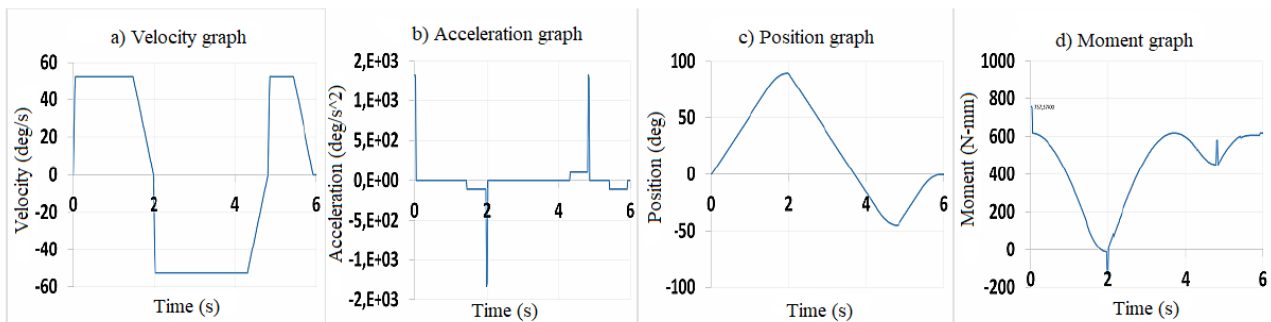


Figure 8. Results obtained by dynamic simulation of the third joint using a Futaba S9206 servomotor. Profile: (a) velocity, (b) acceleration, (c) position and (d) moment. Source: self compiled.

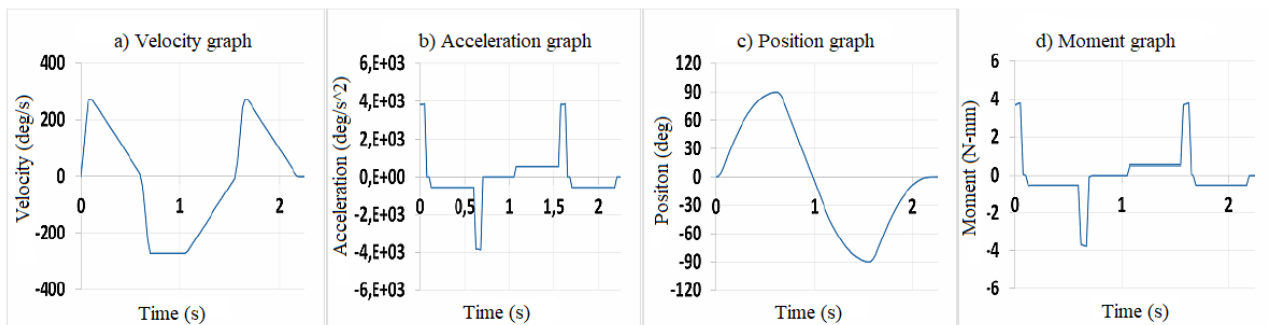


Figure 9. Results obtained by dynamic simulation for the servomotor coupled to the fourth joint (HS-225BB). Profile: (a) Speed, (b) acceleration, (c) position and (d) moment. Source: self compiled.

These analyses are performed at each redesign stage and then optimize the part by removing mass in areas with low stress concentrations. Therefore, quality is eliminated according to three criteria: 1) obtain the minimum safety factor of parts; 2) reduce quality by ensuring that the resulting parts can be manufactured with available machines and tools; 3) the quality of the parts should be low enough to ensure that the actuator can move the arm with the working load.

In most linkage mechanisms, the mass reduction does not reach the ideal safety factor. In this case, the criterion limiting the reduction of quality is the feasibility of part manufacturing, because if the

quality of connecting rod is further reduced, the manufacturing process will become cumbersome and expensive. Therefore, for example, the stress analysis of connecting rod 2 (**Figure 10**) shows that the von Mises stress is 9961 Mpa, the maximum displacement is 0.01631 mm, and the safety factor is greater than 15. Conversely, the stress analysis of connecting rod 3 (**Figure 11**) produced a von Mises stress of 8676 Mpa, with a maximum displacement of 0.006846 mm and a safety factor greater than 15.

On the other hand, the manufacturing of other parts, such as joint shafts, if they allow appropriate quality reduction according to the proposed optimization criteria. For example, the stress analysis of the

horizontal axis of joint 3 corresponding to the belt drive system (Figure 12) shows that the von Mises

stress is 191.9 Mpa, the maximum displacement is 0.1592 mm, and the safety factor is 1.43.

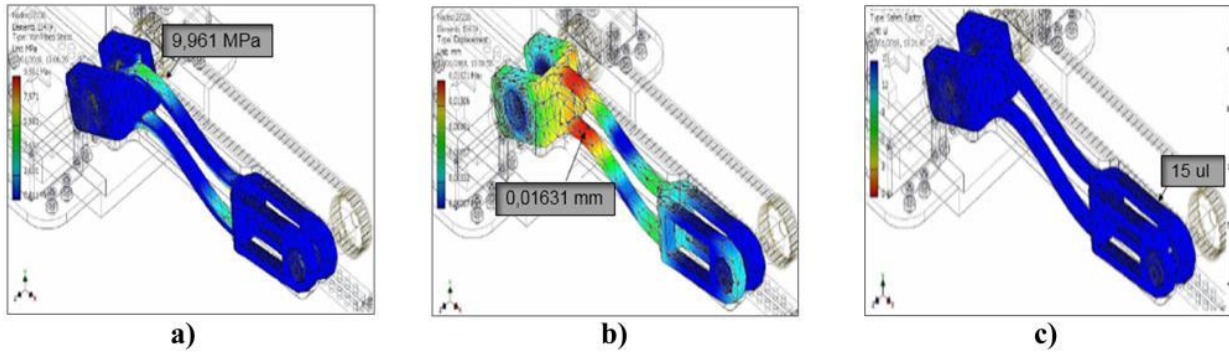


Figure 10. Stress analysis of link 2: (a) von Mises effort, (b) displacement and (c) safety factor. Source: self compiled.

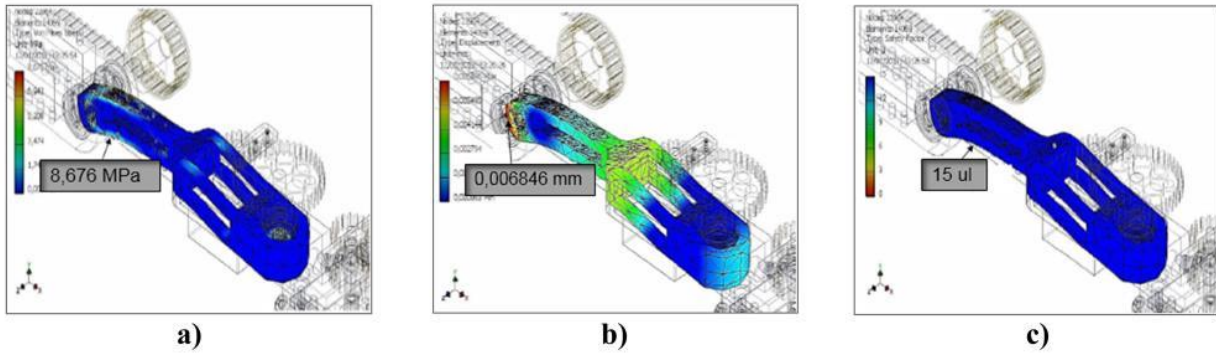


Figure 11. Stress analysis of link 3: (a) on Mises effort, (b) displacement and (c) safety factor. Source: self compiled.

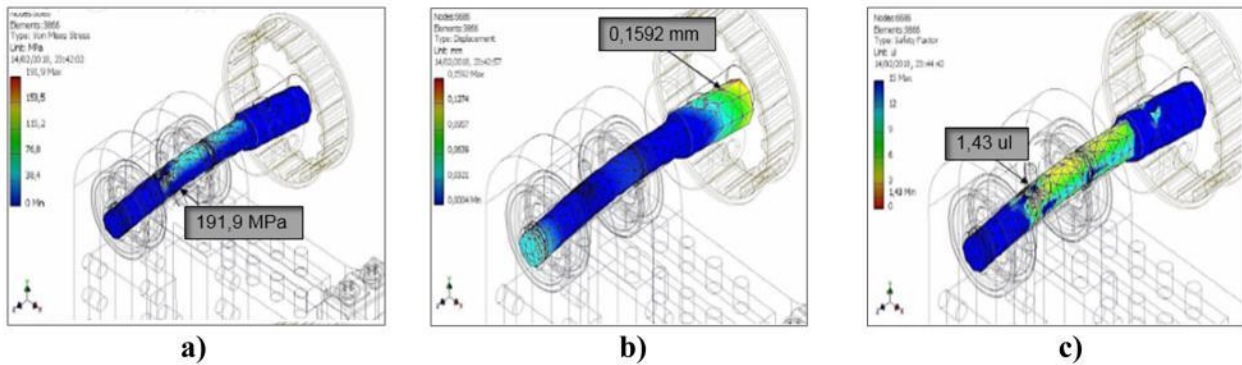


Figure 12. Stress analysis of horizontal axis of joint 3: (a) von Mises effort, (b) displacement and (c) safety factor. Source: self compiled.

3.5 Kinematics model of straight arm

The direct kinematics research is carried out according to the formula of Denavit-Hartenberg^[20], which verifies the simulation using the calculation tool. The first step is to specify a reference system for each joint (Figure 13). From this, a set of equations are derived, which allow the arm joint variables with known end effector position and direction to be

obtained (Table 6). The direct kinematics solution is determined by (3) matching the elements of matrix T with the elements generated by the product of homogeneous transformation matrix:

$$T_0^4 = \begin{bmatrix} n_x & o_x & a_x & p_x \\ n_y & o_y & a_y & p_y \\ n_z & o_z & a_z & p_z \\ 0 & 0 & 0 & 1 \end{bmatrix} = A_1^0 \cdot A_2^1 \cdot A_3^2 \cdot A_4^3 \quad (3)$$

From the matching term to the matching term, equations (4) to (12) are obtained, which correspond to the direction matrix elements of the end effector relative to the reference system at the bottom of the structure; And equations (13) to (15), corresponding to the vector position element of the end effector end relative to the reference system fixed at the bottom of the structure:

Table 6. D-H parameters of mechanical structure

Joint	θ_i	d_i (mm)	a_i (mm)	α_i
1	θ_1	$l_1 = 90$	0	90°
2	θ_2	0	$l_2 = 203.2$	0°
3	θ_3	0	$l_3 = 123.66$	-90°

4 θ_4 0 $L_4 = 114.20$ 0

Source: self compiled.

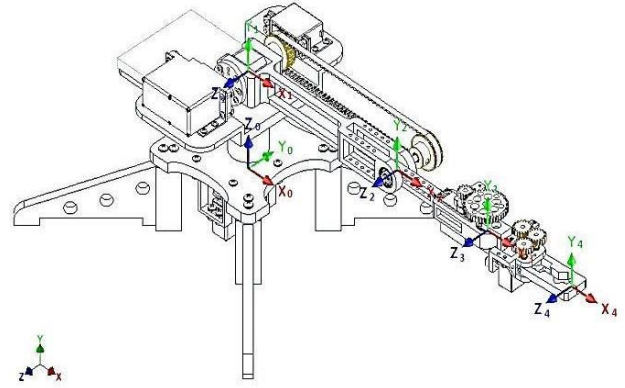


Figure 13. The reference system obtained by Denavit-Hartenberg formula. Source: self compiled.

$$n_x = \cos \theta_1 \cos \theta_2 \cos \theta_3 \cos \theta_4 - \cos \theta_1 \sin \theta_2 \sin \theta_3 \cos \theta_4 - \sin \theta_1 \sin \theta_4 \quad (4)$$

$$n_y = \sin \theta_1 \cos \theta_2 \cos \theta_3 \cos \theta_4 - \sin \theta_1 \sin \theta_2 \sin \theta_3 \cos \theta_4 + \cos \theta_1 \sin \theta_4 \quad (5)$$

$$n_z = \sin \theta_2 \cos \theta_3 \cos \theta_4 + \cos \theta_2 \sin \theta_3 \cos \theta_4 \quad (6)$$

$$o_x = -\cos \theta_1 \cos \theta_2 \cos \theta_3 \sin \theta_4 + \cos \theta_1 \sin \theta_2 \sin \theta_3 \sin \theta_4 - \sin \theta_1 \cos \theta_4 \quad (7)$$

$$o_y = -\sin \theta_1 \cos \theta_2 \cos \theta_3 \sin \theta_4 + \sin \theta_1 \sin \theta_2 \sin \theta_3 \sin \theta_4 + \cos \theta_1 \cos \theta_4 \quad (8)$$

$$o_z = -\sin \theta_2 \cos \theta_3 \sin \theta_4 - \cos \theta_2 \sin \theta_3 \sin \theta_4 \quad (9)$$

$$a_x = -\cos \theta_1 \cos \theta_2 \sin \theta_3 - \cos \theta_1 \sin \theta_2 \cos \theta_3 \quad (10)$$

$$a_y = -\sin \theta_1 \cos \theta_2 \sin \theta_3 - \sin \theta_1 \sin \theta_2 \cos \theta_3 \quad (11)$$

$$a_z = -\sin \theta_2 \sin \theta_3 - \cos \theta_2 \cos \theta_3 \quad (12)$$

$$p_x = \cos \theta_1 \cos \theta_2 (l_4 \cos \theta_3 \cos \theta_4 + l_3 \cos \theta_3) - \cos \theta_1 \sin \theta_2 (l_4 \sin \theta_3 \cos \theta_4 + l_3 \sin \theta_3) - l_4 \sin \theta_1 \sin \theta_4 + l_2 \cos \theta_1 \cos \theta_2 \quad (13)$$

$$p_y = \sin \theta_1 \cos \theta_2 (l_4 \cos \theta_3 \cos \theta_4 + l_3 \cos \theta_3) - \sin \theta_1 \sin \theta_2 (l_4 \sin \theta_3 \cos \theta_4 + l_3 \sin \theta_3) + l_4 \cos \theta_1 \sin \theta_4 + l_2 \sin \theta_1 \cos \theta_2 \quad (14)$$

$$p_z = \sin \theta_2 (l_4 \cos \theta_3 \cos \theta_4 + l_3 \cos \theta_3) + \cos \theta_2 (l_4 \sin \theta_3 \cos \theta_4 + l_3 \sin \theta_3) + l_2 \sin \theta_2 + l_1 \quad (15)$$

3.6 Inverse kinematics model

The inverse kinematics is studied by using the geometric method, and the expressions (16) to (25) suitable for determining the joint variables θ_1 , θ_2 , θ_3 and θ_4 , known the orientation of the end of the structure $\bar{n} = [n_x \ n_y \ n_z]$, and its position $\bar{r}_p = [p_x \ p_y \ p_z]$. For this purpose, we first obtained use θ_1 using the equation (16):

$$\theta_1 = \tan^{-1} \frac{m_y}{m_x} \quad (16)$$

where m_y and m_x are components of the vector \bar{r}_m that was calculated by (17):

$$\begin{aligned} \bar{r}_m &= \bar{r}_p - l_4 \cdot \bar{n} = \begin{bmatrix} m_x & m_y & m_z \end{bmatrix} \bar{r}_m = \bar{r}_p - \\ l_4 \cdot \bar{n} &= \begin{bmatrix} m_x & m_y & m_z \end{bmatrix} \end{aligned} \quad (17)$$

Then, θ_3 was calculate by (18):

$$\theta_3 = \tan^{-1} \frac{\pm \sqrt{1 - \cos^2 \theta_3}}{\cos \theta_3} \quad (18)$$

where $\cos \theta_3$ was obtained through (19), for $\theta_1 = 0^\circ$:

$$\cos \theta_3 = \frac{\left(\frac{m_x}{\cos \theta_1}\right)^2 + (m_z - l_i)^2 - l_2^2 - l_3^2}{2 \cdot l_2 l_3} \quad (19)$$

Or through (20), for $\theta_1 \neq 0^\circ$:

$$\cos \theta_3 = \frac{\left(\frac{m_y}{\sin \theta_1}\right)^2 + (m_z - l_i)^2 - l_2^2 - l_3^2}{2 \cdot l_2 l_3} \quad (20)$$

Then, two characteristic solutions of θ_2 were obtained for the geometry employed; these solutions

are best referred to as “upper elbow solutions” and “lower elbow solutions”:

For $\theta_1 = 0^\circ$ (elbow upward (+); elbow down (-)):

$$\theta_2 = \tan^{-1} \frac{m_z - l_1}{\frac{m_x}{\cos \theta_1}} \pm \tan^{-1} \frac{l_3 \sin \theta_3}{l_2 + l_3 \cos \theta_3} \quad (21)$$

For $\theta_1 \neq 0^\circ$, (elbow upward (+); elbow down (-)):

$$\theta_2 = \tan^{-1} \frac{m_z - l_1}{\frac{m_y}{\sin \theta_1}} \pm \tan^{-1} \frac{l_3 \sin \theta_3}{l_2 + l_3 \cos \theta_3} \quad (22)$$

Finally, calculate θ_4 through (23):

$$\theta_4 = \tan^{-1} \frac{\pm \sqrt{1 - \cos^2 \theta_4}}{\cos \theta_4} \quad (23)$$

where $\cos \theta_4$ was obtained through (24):

$$\cos \theta_4 = \frac{r_p^2 - d_4^2 - r_m^2}{2d_4 r_m} \quad (24)$$

And:

r_m = Module of the position vector \bar{r}_m

r_p = Module of the position vector \bar{r}_p

d_4 = Module of the position vector \bar{d}_4 , calculated by (25):

$$d_4 = |\bar{r}_p - \bar{r}_m| \quad (25)$$

3.7 Workload structure

The calculation workload of the robot arm (**Figure 14**) is obtained by considering the joint limit (**Table 7**) and the maximum range in the design due to the mechanical buffer in the servo motor. The

maximum range is defined by the farthest point at which the arm can locate its end actuator. In this case, the maximum range is 450 mm. The workload calculated for the final design is: $V_{Trabajo} = 0.02965 m^3$. Since the use of a gear transmission system with a gear ratio of 2.8 limits the variable to only the opening, the first joint mainly limits the variable θ_1 to only 64° , but as mentioned above, this transmission is necessary to ensure that the actuator is effective during startup, thus helping to implement an appropriate control system.

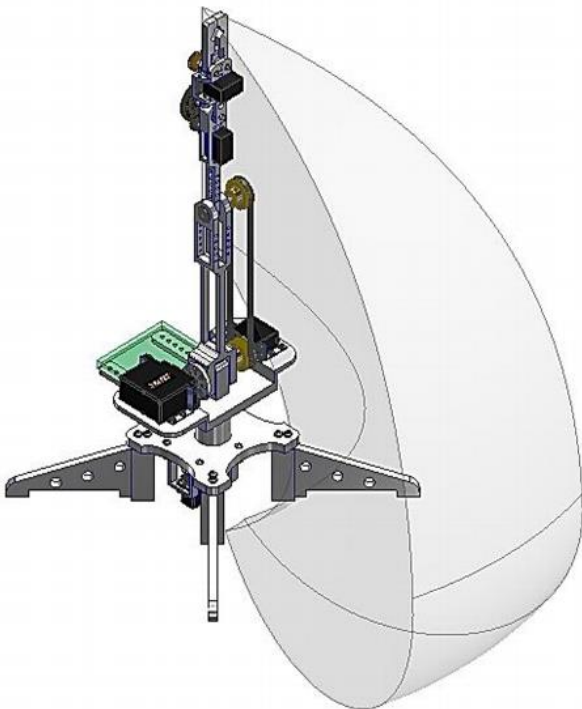


Figure 14. The workload of the robot arm. Source: self compiled.

3.8 Final design and construction of the structure

Finally, the assembly process of each component of the robot arm is completed. These materials are made of aluminum by casting process. After casting, the parts are refined by machining to obtain an acceptable surface finish. Finally, the result obtained was a robotic arm that conforms to the design made in Autodesk Inventor® software and to the product specifications initially established (**Figure 15**).

Table 7. The joint boundary on the robot arm

Joint	Servo-motor	Variable	Minimum value	Maximum value
1	HS-322H D	θ_1	-32°	32°
2	HS-805B B	θ_2	0°	180°
3	Fukuda S9206	θ_3	-45°	90°
4	HS-225B B	θ_4	30°	30°

Source: self compiled.



Figure 15. Robotic arm built. Source: self compiled.

4. Discussion

The designed manipulator is developed according to the product specifications determined by customers. In this regard, the design fully meets the required indicators, all of which are higher than the set threshold: the workload is initially estimated to be at least 0.05 kg; after the design process, it is determined that the actual working load is 0.1 kg, which is higher than the minimum allowable value. The maximum range of the arm is estimated to be at least 0.4 meters; during the design process, the total range of 0.45 m was determined, which was also higher than the minimum allowable value. The total mass of the structure has been determined to be less than 6 kg, but the final structural mass is 3.2 kg, which effectively realizes the basic purpose of reducing mass and easy to move equipment. The time required for periodic maintenance is set to $\frac{1}{2}$ hours (theoretically according to the modular definition of arm).

In addition, a wrist that allows the exchange of end effectors is designed, and a built-in device with good appearance is obtained. In all cases, the safety factor of parts is greater than 1.2, forming a structure

within the range of established parameters. It must be pointed out that the safety factor of some parts is greater than 15; this value supports the idea of continuing the quality reduction process, but considering the limitations of the existing manufacturing process, it is decided not to continue to redesign the parts. Finally, the required workload is 0.01 m³. The actual value is 0.02965 m³, higher than expected.

5. Conclusion

This paper introduces a design method of robot arm, which includes defining 12 design specifications according to customer requirements. Six design concepts are generated and evaluated according to two evaluations: one is qualitative and the other is quantitative. The concept that can best meet the initially proposed customer needs is obtained.

The size and optimization of each arm component are based on three criteria: the minimum safety factor of each component, the manufacturing feasibility of available machines and tools, and the appropriate quality to ensure the capability of the actuator. This process is realized through two types of analysis and calculation tools: mechanical event simulation (dynamic simulation) to obtain the maximum load and torque of each component when following the critical trajectory; the stress analysis is carried out by finite element method, especially at the critical position of high load and high bending moment. After seven iterations, the size of each part was modified and evaluated according to the above two analyses, and a low-quality optimized structure meeting the defined criteria was obtained.

In addition, dynamic simulations were performed to verify that the torque applied by the actuator was sufficient to move along all possible trajectories on the required speed profile.

In addition, the direct kinematics modeling is carried out by using Denavit-Hartenberg formula, and the inverse kinematics modeling is carried out by using geometric method. By comparing the application results with the results obtained by computer simulation, the obtained equation is verified. The simulation allows the CAD model of the arm to be established with different joint variable

values to determine the final position and direction of the arm. It also defines the transmission ratio, joint boundary and workload at the joint according to the structural characteristics of the actuator, which also meet the expected volume.

The structure of the manipulator is established and assembled with aluminum as the constitutive material and casting and machining as the manufacturing process. The obtained structure meets the size and quality requirements determined in the previous design stage. Finally, it must be pointed out that the future work aims to develop the electronic structure, architecture and control system of arm debugging.

Conflict of interest

Authors declared no conflict of interest.

Acknowledgement

This work is financed by the Dean's Office of Research, Universidad Nacional Experimental del Táchira, under project 01-009-2017.

References

1. Barraza Cantillo A, Rúa Charris J, Sosa Rodríguez J, *et al.* Modelado dinámico del manipulador serial Mitsubishi Movemaster RV-M1 usando SolidWorks [Dynamic modeling of Mitsubishi Movemaster RV-M1 serial manipulator using SolidWorks]. Revista UIS Ingenierías 2016; 15(2): 49-62. doi: 10.18273/revuin.v15n2-2016004.
2. Iqbal J, Khan Z, Khalid A. Prospects of robotics in food industry. Food Science and Technology 2017; 37(2): 159-165. doi: 10.1590/1678-457X.14616.
3. Ceballos E, Díaz-Rodríguez M, Paredes J, *et al.* Desarrollo de un robot de rehabilitación pasiva para la articulación de la muñeca mediante la implementación de un microcontrolador Arduino UNO [Development of a passive rehabilitation robot for wrist joint by implementing an Arduino UNO microcontroller]. Revista UIS Ingenierías 2017; 16(1): 59-68.
4. Feng Q, Wang X, Zheng W, *et al.* New strawberry harvesting robot for elevated-trough culture. International Journal of Agricultural Bioengineering 2012; 5(2): 1-8. doi: 10.3965/j.ijabe.20120502.001.

5. Lindemann RA, Bickler DB, Harrington BD, *et al.* Mars exploration rover mobility development. *IEEE Robotic & Automation Magazine* 2006; 13(2): 19-26. doi: 10.1109/MRA.2006.1638012.
6. García-Cerezo A, Mandow A, Martínez JL, *et al.* Development of ALACRANE: A mobile robotic assistance for exploration and rescue missions. 2007 IEEE International Workshop on Safety, Security and Rescue Robotics; Rome. 2007; p. 1-6.
7. Guarnieri M, Kurazume R, Masuda H, *et al.* HELIOS system: A team of tracked robots for special urban search and rescue operations. 2009 IEEE/RSJ International Conference on Intelligent Robots and Systems; 2009 Oct 10-15; St. Louis, MO, USA. IEEE; 2009; p. 2795-2800. doi: 10.1109/IROS.2009.5354452.
8. Brooks L. Adventures in liquid space: Representations of the sea in Disney theme parks. In: Hackett J, Harrington S (editors). *Beasts of the Deep: Sea Creatures and Popular Culture*. Harrington: John Libby Publishing Co., Ltd.; 2018. p. 142-154.
9. Balmori G. Cine y robots: del autómatas al androide [Film and robot: From automata to robot]. *Revista de Occidente* 2017; 436: 85-96.
10. Cárdenas P, Parreño R. Diseño e implementación del sistema de control y audio de la maqueta animada del Allosaurio para el Museo de Historia Natural Gustavo Orcés V [Design and implementation of the control and audio system for the animated model of the Allosaurus for the Gustavo Orcés V Museum of Natural History] [thesis]. Quito: Escuela Politécnica Nacional; 2018.
11. Barrera N. Uso de la robótica educativa como estrategia didáctica en el aula [Use of educational robotics as a didactic strategy in the classroom]. *Praxis & Saber* 2015; 6(11): 215-234. doi: 10.19053/22160159.3582.
12. Moreno I, Muñoz L, Serracín JR, *et al.* Robotic education, a tool for the teaching-learning of the science and technology. *Teoría de la Educación. Educación y Cultura en la Sociedad de la Información* 2012; 13(2): 74-90.
13. Batz CRB. Diseño y construcción de un brazo robótico [Design and construction of a robotic arm] [thesis]. Guatemala: Universidad de San Carlos de Guatemala; 2005.
14. Martínez G, Jáquez S, Rivera J, *et al.* Diseño propio y construcción de un brazo robótico de 5 GDL [In-house design and construction of a 5 GDL robotic arm]. *Revista de Ingeniería Eléctrica, Electrónica y Computación* 2008; 4(1): 1-7.
15. Mahendrakumar MA, Patel PD, Bhagubhai VT, *et al.* Design and development of pick and place robotics arm using PLC-Scada. *International Conference on Current Research in Engineering*; 2017 Apr 13; Gujarat, India. 2017. p. 1-7.
16. Riano-Jaimes C, Peña-Cortés C, Sánchez-Acevedo H. Aplicación de técnicas de desenvolvimiento de producto para el desarrollo de un robot antropomórfico [Application of product development techniques for the development of an anthropomorphic robot]. *Revista UIS Ingenierías* 2018; 17(1): 21-34. doi: 10.18273/revuin.v17n1-2018002.
17. Jabonero J. Modelado y Análisis de un Brazo Mecánico [Modeling and Analysis of a Mechanical Arm] [thesis]. Carlos Madrid: Universidad Carlos III de Madrid; 2010.
18. Ulrich K, Eppinger S. Diseño y desarrollo de productos, Cuarta educupib [Product design and development]. 4th ed. Mexico: McGraw-Hill/Interamericana editors; 2013.
19. Braun J. Libro de formulas [Book of formulas]. Sachseln: Editorial maxon academy; 2013.
20. Blanco J. Parametrización Denavit-Hartenberg para robots: Teoría, vídeo y nueva aplicación libre [Denavit-Hartenberg parameterization for robots: Theory, video and free new application] [Video]. February 2013. Available from: <https://www.cienciaexplicada.com/2013/02/parametrizacion-denavithartenberg-para.html>.
21. Jaramillo A. Cinemática de manipuladores robóticos.2005 [Kinematics of manipulators robotic manipulators.2005] [Internet]. Available from: http://www.wag.caltech.edu/home/ajaramil/libro_robotica/cinematica.pdf.